Astronomy & Astrophysics manuscript no. fams
March 27, 2012

Constraining the cometary flux through the asteroid belt during the Late Heavy Bombardment

M. Brož[1], A. Morbidelli[2], W.F. Bottke[3], J. Rozehnal[1], D. Vokrouhlický[1], D. Nesvorný[3]

[1] Institute of Astronomy, Charles University, Prague, V Holešovičkách 2, 18000 Prague 8, Czech Republic, e-mail: mira@sirrah.troja.mff.cuni.cz, rozehnal@observatory.cz, davok@cesnet.cz
[2] Observatoire de la Côte d'Azur, BP 4229, 06304 Nice Cedex 4, France, e-mail: morby@oca.eu
[3] Department of Space Studies, Southwest Research Institute, 1050 Walnut St., Suite 300, Boulder, CO 80302, USA, e-mail: bottke@boulder.swri.edu, davidn@boulder.swri.edu

Received ???; accepted ???

ABSTRACT

Context. In the Nice model, the Late Heavy Bombardment (LHB) is related to an orbital instability of giant planets which causes a fast dynamical dispersion of a transneptunian cometary disk (Gomes et al. 2005).
Aims. We study effects produced by these hypothetical cometary projectiles on main-belt asteroids. In particular, we want to check if the observed collisional families provide a lower or an upper limit for the cometary flux during the LHB.
Methods. We present an updated list of observed asteroid families as identified in the space of synthetic proper elements by the hierarchical clustering method, colour data, albedo data and dynamical considerations and we estimate their physical parameters. We select 12 families which may be related to the LHB according to their dynamical ages. We then use collisional models and N-body orbital simulations to get insights into long-term dynamical evolution of synthetic LHB families over 4 Gyr. We account for mutual collisions between comets, main-belt asteroids and family members, physical disruptions of comets, the Yarkovsky/YORP drift in semimajor axis, chaotic diffusion in eccentricity/inclination, or possible perturbations by the giant-planet migration.
Results. Assuming a "standard" size-frequency distribution of primordial comets, we predict the number of families with parent body sizes $D_{\rm PB} \geq 200$ km – created during the LHB and subsequent $\simeq 4$ Gyr of collisional evolution – which seems consistent with observations. However, more than 100 asteroid families with $D_{\rm PB} \geq 100$ km should be created at the same time which are not observed. This discrepancy can be nevertheless explained by the following processes: i) asteroid families are efficiently destroyed by comminution (via collisional cascade), ii) disruptions of comets below some critical perihelion distance ($q \lesssim 1.5$ AU) are common.
Conclusions. Given the freedom in the cometary-disruption law, we cannot provide stringent limits on the cometary flux, but we can conclude that the observed distribution of asteroid families is not in contradiction with a cometary LHB.

Key words. celestial mechanics – minor planets, asteroids: general – comets: general – methods: numerical

1. Introduction

The Late Heavy Bombardment (LHB) is an important period in the history of the solar system. It is often defined as the process that made huge but relatively young impact basins (a 300 km or larger diameter crater) on the Moon like Imbrium and Orientale. The sources and extent of the LHB, however, has been undergoing recent revisions. In the past, there were two end-member schools of thought describing the LHB. The first school argued that nearly all lunar basins, including the young ones, were made by impacting planetesimals leftover from terrestrial planet formation (Neukum et al. 2001, Hartmann et al. 2000, 2007; see Chapman et al. 2007 for a review). The second school argued that most lunar basins were made during a spike of impacts which took place near 3.9 Ga (e.g., Tera et al. 1974, Ryder et al. 2000).

Recent studies, however, suggest that a compromise scenario may be the best solution: the oldest basins were mainly made by leftover planetesimals, while the last 12–15 or so lunar basins were created by asteroids driven out of the primordial main belt by the effects of late giant-planet migration (Tsignais et al. 2005, Gomes et al. 2005, Minton & Malhotra 2009, Morbidelli et al. 2010, Marchi et al. 2012, Bottke et al. 2012). This would mean the LHB is limited in extent; it does not encompass all lunar basins. If this view is correct, we can use studies of lunar and asteroid samples heated by impact events, together with dynamical modeling work, to suggest that the basin-forming portion of the LHB lasted from approximately 4.1–4.2 to 3.7–3.8 billion years ago on the Moon (Bogard 1995, 2011, Swindle et al. 2009, Bottke et al. 2012, Norman & Nemchin 2012).

The so-called 'Nice model' provides a coherent explanation of the origin of the LHB as an impact spike or rather a "saw-tooth" (Morbidelli et al. 2012). According to this model, the bombardment was triggered by a late dynamical orbital instability of the giant planets, in turn driven by the gravitational interactions between said planets and a massive trans-Neptunian disk of planetesimals (see Morbidelli 2010 for a review). In this scenario, three projectile populations contributed to the LHB: the comets from the original trans-Neptunian disk (Gomes et al. 2005), the asteroids from the main belt (Morbidelli et al. 2010) and those from a putative extension of the main belt towards Mars, inwards of its current inner edge (Bottke et al. 2012). The latter could have been enough of a source for the LHB, as recorded in the lunar crater record (Bottke et al. 2012), while the asteroids from the current main belt boundaries would have been only a minor contributor (Morbidelli et al. 2010).

The Nice model, however, predicts a very intense cometary bombardment of which there seems to be no obvious traces on

the Moon. In fact, given the expected total mass in the original trans-Neptunian disk (Gomes et al. 2005) and the size distribution of objects in said disk (Morbidelli et al. 2009), the Nice model predicts that about 5×10^4 km-size comets should have hit the Moon during the LHB. This would have formed 20 km craters with a surface density of 1.7×10^{-3} craters per km^2. But the highest crater densities of 20 km craters on the lunar highlands is less than 2×10^{-4} (Strom et al. 2005). This discrepancy might be explained by a gross overestimate of the number of small bodies in the original trans-Neptunian disk in Morbidelli et al. (2009). However, all impact clast analyses of samples associated to major LHB basins (Kring and Cohen 2002, Tagle 2005) show that also the major projectiles were not carbonaceous chondrites or similar primitive, comet-like objects.

The lack of evidence for a cometary bombardment of the Moon can be considered as a fatal flaw of the Nice model. Curiously, however, in the outer solar system we see evidence for the cometary flux predicted by the Nice model. Such a flux is consistent with the number of impact basins on Iapetus (Charnoz et al. 2009), with the number and the size distribution of the irregular satellites of the giant planets (Nesvorný et al. 2007, Bottke et al. 2010) and of the Trojans of Jupiter (Morbidelli et al. 2005), as well as with the capture of D-type asteroids into the outer asteroid belt (Levison et al., 2009). Moreover, the Nice model cometary flux is required to explain the origin of the collisional break-up of the asteroid (153) Hilda in the 3/2 resonance with Jupiter (located at $\simeq$ 4 AU, i.e. beyond the nominal outer border of the asteroid belt at $\simeq$ 3.2 AU; Brož et al. 2011).

Missing signs of an intense cometary bombardment on the Moon and the evidence for a large cometary flux in the outer solar system suggests that the Nice model may be correct in its basic features, but most comets disintegrated as they penetrated deep into the inner solar system.

To support or reject this possibility, this paper focuses at the main asteroid belt, looking for constraints on the flux of comets through this region at the time of the LHB. In particular we focus on old asteroid families, produced by the collisional break-up of large asteroids, which may date back at the LHB time. We provide a census of these families in Section 2.

In Section 3, we construct a collisional model of the main belt population. We show that, on average, this population alone could not have produced the observed number of families with $D_{\rm PB}$ = 200–400 km. Instead, the required number of families with large parent bodies is systematically produced if the asteroid belt was crossed by a large number of comets during the LHB, as expected in the Nice model (see Section 4). However, for any reasonable size distribution of the cometary population, the same cometary flux that would produce the correct number of families with $D_{\rm PB}$ = 200–400 km, would produce too many families with $D_{\rm PB} \simeq 100$ km relative to what is observed. Therefore, in the subsequent sections we look for mechanisms that might prevent detection of most of these families.

More specifically, in Sec. 5 we discuss the possibility that families with $D_{\rm PB} \simeq 100$ km are so numerous that they cannot be identified because they overlap with each other. In Sec. 6 we investigate their possible dispersal below detectability due to the Yarkovsky effect and chaotic diffusion. In Sec. 7 we discuss the role of physical lifetime of comets. In Sec. 8 we analyze the dispersal of families due to the changes in the orbits of the giant planets expected in the Nice model. In Sec. 9 we consider the subsequent collisional comminution of the families. Of all investigated processes, the last one seems to be the most promising to reduce the number of visible families with $D_{\rm PB} \simeq 100$ km while not affecting the detectability of old families with $D_{\rm PB}$ = 200–400 km.

Finally, in Section 10 we analyze a curious portion of the main belt, located in a narrow semi-major axis zone bounded by the 5:2 and 7:3 resonances with Jupiter. This zone is severely deficient in small asteroids compared to the other zones of the main belt. For the reasons explained in the section, we think that this zone best preserves the initial asteroid belt population, and therefore we call it the "pristine zone". We check the number of families in the pristine zone, their sizes and ages and find that they are consistent with the number expected in our model invoking a cometary bombardment at the LHB time and a subsequent collisional comminution and dispersion of the family members.

The conclusions follow in Section 11.

2. A list of known families

Although there exist several lists of families in the literature (Zappalá et al. 1995, Nesvorný et al. 2005, Parker et al. 2008, Nesvorný 2010) we are going to identify families once again. The reason is that we seek an *upper limit* for the number of *old families* which may be significantly dispersed and depleted, while the previous works often focused on well defined families. Moreover, we need to calculate several *physical parameters* of the families (like the parent-body size, slopes of the size-frequency distribution, a dynamical age estimate if not available in the literature) which are crucial for further modelling. Last but not least, we use more precise *synthetic* proper elements from the AstDyS database (Knežević & Milani 2003) instead of semi-analytic ones.

We employ a hierarchical clustering method (HCM, Zappalá et al. 1995) for the *initial* identification of families in the proper element space $(a_{\rm p}, e_{\rm p}, \sin I_{\rm p})$, but then we have to perform a lot of manual operations, because: i) we have to select a reasonable cut-off velocity $v_{\rm cutoff}$, usually such that the number of members $N(v_{\rm cutoff})$ increases relatively slowly with increasing $v_{\rm cutoff}$. ii) The resulting family should also have a "reasonable" shape in the space of proper elements which should somehow correspond to the local dynamical features.[1] iii) We check taxonomic types (colour indices from the Sloan DSS MOC catalogue version 4, Parker et al. 2008) which should be consistent among family members. We can recognise interlopers or overlapping families this way. iv) Finally, the size-frequency distribution should exhibit one or two well-defined slopes, otherwise the cluster is considered uncertain.

Our results are summarised in online Tables 1–3 and the positions of families within the main belt are plotted in Figure 1. Note that our list is "optimistic", so that even not-so-prominent families are included here.[2]

There are however several potential problems we are aware of:

1. There may exist *inconsistencies* among different lists of families. For example, sometimes a clump may be regarded as a single family or as two separate families. This may be the case of: Padua and Lydia, Rafita and Cameron.

[1] For example, the Eos family has a complicated but still reasonable shape, since it is determined by several intersecting high-order mean-motion or secular resonances, see Vokrouhlický et al. (2006).

[2] On the other hand, we do not include all of the small and less-certain clumps in high-inclination region as listed by Novaković et al. (2011). Anyway, we do not focus on small or high-I families in this paper.

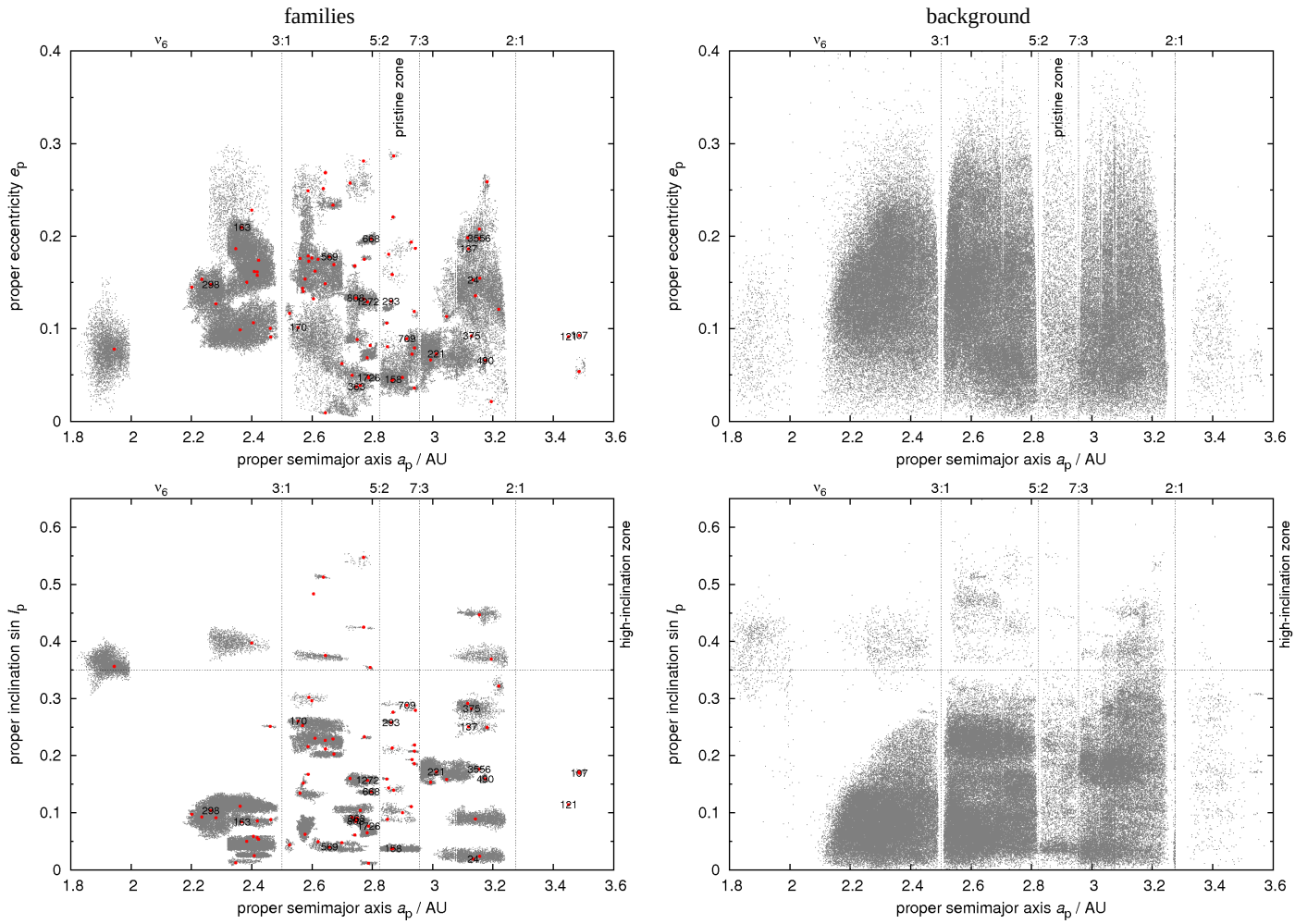

Fig. 1. Asteroids from the synthetic AstDyS catalogue plotted in the proper semimajor axis a_p vs proper eccentricity e_p (top panels) and a_p vs proper inclination sin I_p planes (bottom panels). We show the identified asteroid families (left panels) with the positions of the largest members indicated by red symbols, and also remaining background objects (right panels). The labels correspond to designations of asteroid families which we focus on in this paper. Note that there are still some structures consisting of *small* objects in the background population, visible only in the inclinations (bottom right panel). These "halos" may arise from two reasons: (i) a family has no sharp boundary and its transition to the background is smooth, or (ii) there are bodies escaping from the families due to long-term dynamical evolution. Nevertheless, we checked that these halo objects do not significantly affect our estimates of parent-body sizes.

2. For the identification of families we use *synthetic* proper elements, which are more precise than the semi-analytic ones. Sometimes the families look more regular (e.g., Teutonia) or more tightly clustered (Beagle) when we use the synthetic elements. This very choice may however affect results substantially! A clear example is the Teutonia family which contains also the *big* asteroid (5) Astraea if the synthetic proper elements are used, but *not* if the semi-analytic proper elements are used. This is due to the large differences between the semi-analytic and synthetic proper elements of (5) Astraea. Consequently, the physical properties of the two families differ considerably. We believe that the family defined from the synthetic elements is more reliable.
3. Durda et al. (2007) often claim *larger* size of the parent body (e.g., Themis, Meliboea, Maria, Eos, Gefion, Baptistina), because they try to match the SFD of larger bodies and the results of SPH experiments. This way they account also for small bodies which existed at the time of the disruption, but which do *not* exist today since they were lost due to collisional grinding and the Yarkovsky effect. We prefer to use $D_{\rm Durda}$ instead of value $D_{\rm PB}$ estimated from the currently observed SFD.

2.1. A definition of the production function

In order to compare observed families to simulations, we define a "production function" as the cumulative number $N(>D)$ of families with parent-body size $D_{\rm PB}$ larger than given D. The observed production function is shown in Figure 2 and it is worth to note that it is very shallow. The number of families with $D_{\rm PB} \simeq 100$ km is comparable to the number of families in the $D_{\rm PB} = 200$–400 km range.

It is important to note that the observed production function is likely to be affected by biases (the family sample may not be complete, especially below $D_{\rm PB} \lesssim 100$ km) and also by long-term collisional/dynamical evolution which may prevent a detection of old comminutioned/dispersed families today (Marzari et al. 1999).

From the theoretical point of view, the slope q of the production function $N(>D) \propto D^q$ should correspond to the cumulative

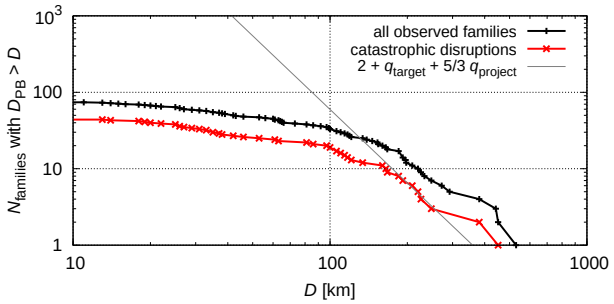

Fig. 2. A production function (i.e. the cumulative number $N(>D)$ of families with parent-body size $D_{\rm PB}$ larger than D) for all observed families (black) and families corresponding to catastrophic disruptions (red), i.e. with largest remnant/parent body ratio smaller than 0.5. We also plot a theoretical slope according to Eq. (1), assuming $q_{\rm target} = -3.2$ and $q_{\rm project} = -1.2$ which correspond to the slopes of the main belt population in the range $D = 100$–200 km and $D = 15$–60 km, respectively.

slopes of the size-frequency distributions of the target and projectile populations. It is easy to show[3] that the relation is

$$q = 2 + q_{\rm target} + \frac{5}{3} q_{\rm project} \,. \qquad (1)$$

Of course, real populations may have complicated SFD's, with different slopes in different ranges. Nevertheless, any populations which have a steep SFD's (e.g. $q_{\rm target} = q_{\rm project} = -2.5$) would inevitably produce a steep production function ($q \doteq -4.7$).

In the following analysis, we drop cratering events and we discuss catastrophic disruptions only, i.e. families which have largest remnant/parent body ratio smaller than 0.5. The reason is that the same criterion LR/PB < 0.5 is used in collisional models. Moreover, cratering events were not yet systematically explored by SPH simulations due to insufficient resolution (Durda et al. 2007).

2.2. Methods for family age determination

If there is no previous estimate of the age of a family, we use one of the following three dynamical methods to determine it: i) a simple $(a_{\rm p}, H)$ analysis as in Nesvorný et al. (2005); ii) a C-parameter distribution fitting as introduced by Vokrouhlický et al. (2006); iii) a full N-body simulation described e.g. in Brož et al. (2011).

In the first approach, we assume zero initial velocities and the current extent of the family is explained by the size-dependent Yarkovsky semimajor axis drift. This way we can obtain only an *upper limit* for the dynamical age, of course. We show an example for the Eos family in Figure 3. The extent of the family in the proper semimajor axis vs the absolute magnitude $(a_{\rm p}, H)$ plane can be described by the parametric relation

$$0.2H = \log_{10} \frac{|a_{\rm p} - a_{\rm c}|}{C} \,, \qquad (2)$$

where $a_{\rm c}$ denotes the centre of the family, and C is the parameter. The limiting value, for which all Eos family members (except interlopers) are *above* the corresponding curve, is $C = 1.5$ to 2.0×10^{-4} AU. Assuming reasonable thermal parameters (summarised in Table 4) we can then calculate the age to be $t < 1.5$ to 2.0 Gyr.

[3] Assuming that the strength is approximately $Q_D^\star \propto D^2$ in the gravity regime, the necessary projectile size $d \propto (Q_D^\star)^{1/3} D$ (Bottke et al. 2005) and the number of disruptions $n \propto D^2 D^{q_{\rm target}} d^{q_{\rm project}}$.

Table 4. Nominal thermal parameters for S and C/X taxonomic types of asteroids: $\rho_{\rm bulk}$ denotes the bulk density, $\rho_{\rm surf}$ the surface density, K the thermal conductivity, $C_{\rm th}$ the specific thermal capacity, $A_{\rm Bond}$ the Bond albedo and ϵ the infrared emissivity.

type	$\rho_{\rm bulk}$ (kg/m^3)	$\rho_{\rm surf}$ (kg/m^3)	K (W/m/K)	$C_{\rm th}$ (J/kg/K)	$A_{\rm Bond}$	ϵ
S	2500	1500	0.001	680	0.1	0.9
C/X	1300	1300	0.01	680	0.02	0.9

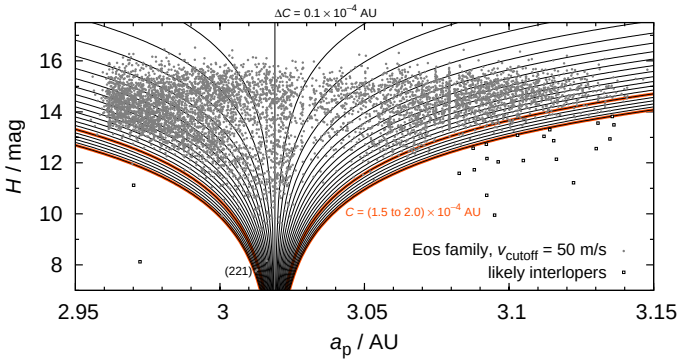

Fig. 3. An example of the Eos asteroid family, shown on the proper semimajor axis $a_{\rm p}$ vs absolute magnitude H plot. We also plot curves defined by the equation (2) and parameters $a_{\rm c} = 3.019$ AU, $C = 1.5$ to 2.0×10^{-4} AU which is related to the upper limit of the dynamical age of the family.

The second method uses a histogram $N(C, C + \Delta C)$ of the number of asteroids with respect to the C parameter defined above, which is fitted by a dynamical model of the initial velocity field and the Yarkovsky/YORP evolution. This enables us to determine the *lower limit* for the age too (so the resulting age estimate is $t = 1.3^{+0.15}_{-0.2}$ Gyr for the Eos family).

In the third case, we start an N-body simulation using a modified SWIFT integrator (Levison and Duncan 1994), with the Yarkovsky/YORP acceleration included, and evolve a synthetic family up to 4 Gyr. We try to match the shape of the observed family in all three proper orbital elements $(a_{\rm p}, e_{\rm p}, \sin I_{\rm p})$. In principle, this method may provide somewhat independent estimate of the age. For example, there is a 'halo' of asteroids in the surroundings of the nominal Eos family, which are of the same taxonomic type K, and we may fit the ratio $N_{\rm halo}/N_{\rm core}$ of the number of objects in the 'halo' and in the family 'core' (Brož et al., in preparation).

The major source of uncertainty in all methods are unknown bulk densities of asteroids (although we use the most likely values for the S or C/X taxonomic classes). The age scales approximately as $t \propto \rho_{\rm bulk}$. Nevertheless, we are still able to distinguish families which are young from those which are old.

2.3. Which families can be of LHB origin?

The ages of the observed families and their parent-body sizes are shown in Figure 4. Because the ages are generally very uncertain, we consider than any family whose nominal age is older than 2 Gyr is potentially a family formed ~4 Gyr ago, i.e. at the LHB time. If we compare the number of "young" (<2 Gyr) and old families (>2 Gyr) with $D_{\rm PB} = 200$–400 km we cannot see a significant over-abundance of old family formation events. On the other hand, we almost do not find any small old families.

Only 12 families from the whole list may be *possibly* dated back to the Late Heavy Bombardment, because their dynamical

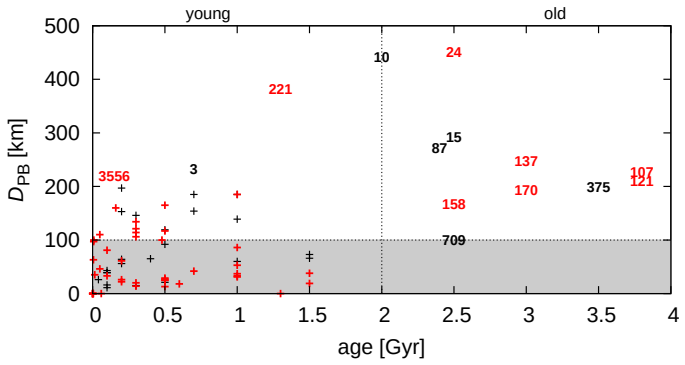

Fig. 4. The relation between dynamical ages of families and the sizes of their parent bodies. Red labels correspond to catastrophic disruptions while cratering events are labelled black. Some of the families are denoted by the designation of the largest member. The uncertainties of both parameters are listed in Tables 1–3 (we do not include overlapping error bars here for clarity).

Table 5. Old families with ages possibly approaching the LHB. They are sorted according to the parent body size, where D_{Durda} determined by the Durda et al. (2007) method is preferred to the estimate D_{PB} inferred from the observed SFD. An additional 'c' letter indicates that we extrapolated the SFD down to $D = 0$ to account for small (unobserved) asteroids, an exclamation mark denotes a significant mismatch between D_{PB} and D_{Durda}.

designation		D_{PB} (km)	D_{Durda} (km)	note
24	Themis	209c	380–430!	
10	Hygiea	410	442	cratering
15	Eunomia	259	292	cratering
702	Alauda	218c	290–330!	high-I
87	Sylvia	261	272	cratering
137	Meliboea	174c	240–290!	
375	Ursula	198	240–280	cratering
107	Camilla	>226	-	non-existent
121	Hermione	>209	-	non-existent
158	Koronis	122c	170–180	
709	Fringilla	99c	130–140	cratering
170	Maria	100c	120–130	

ages approach $\sim$ 3.8 Gyr (including the relatively large uncertainties; see Table 5, which is an excerpt from Tables 1–3).

If we drop cratering events and the families of Camilla and Hermione which do not exist any more today (their existence was inferred from the satellite systems, Vokrouhlický et al. 2010) we end up with *only* 5 families created by catastrophic disruptions which potentially may date from the LHB time (i.e. their nominal age is larger than 2 Gy). As we shall see in Section 4, this is an unexpectedly low number.

Moreover, it is really intriguing that most "possibly-LHB" families are larger than $D_{\mathrm{PB}} \simeq 200$ km. It seems that old families with $D_{\mathrm{PB}} \simeq 100$ km are missing in the observed sample. This is an important aspect which we have to explain, because it contradicts our expectation of a steep production function.

3. Collisions in the main belt alone

Before we proceed to scenarios involving the LHB, we try to explain the observed families with ages spanning 0–4 Gyr as a result of collisions only among main-belt bodies. To this purpose, we used the collisional code called Boulder (Morbidelli et al. 2009) with the following setup: the intrinsic probabilities $P_{\mathrm{i}} = 3.1 \times 10^{-18}\,\mathrm{km}^{-2}\,\mathrm{yr}^{-1}$, the mutual velocities $V_{\mathrm{imp}} = 5.28$ km/s for the MB vs MB collisions (both were taken from the work of Dahlgren 1998). The scaling law is described by the polynomial relation (r denotes radius in cm):

$$Q_D^\star(r) = \frac{1}{q_{\mathrm{fact}}}\left(Q_0 r^a + B\rho r^b\right) \qquad (3)$$

with the parameters corresponding to basaltic material at 5 km/s (Benz & Asphaug 1999):

ρ (g/cm^3)	Q_0 (erg/g)	a	B (erg/g)	b	q_{fact}
3.0	7×10^7	−0.45	2.1	1.19	1.0

We selected the time span of the simulation 4 Gyr (not 4.5 Gyr) since we are interested in this last evolutionary phase of the main belt, when its population and collisional activity is of the same order as today (Bottke et al. 2005). The outcome of a single simulation also depends on the "seed" value of the random-number generator that is used in the Boulder code to decide whether a collision with a fractional probability actually occurs or not in a given time step. We thus have to run multiple simulations to obtain information on this stochasticity of the collisional evolution process.

We use the observed SFD of the main belt as the first constraint for our collisional model. We do *not* use only a single number to describe the number of observed families (e.g. $N = 20$ for $D_{\mathrm{PB}} \geq 100$ km), but we discuss a complete production function instead. The results in terms of the production function are shown in Figure 5 (left column, 2nd row). On average, the synthetic production function is steeper and *below* the observed one, even though there is approximately a 5 % chance that a single realization of the computer model would resemble the observations quite well. This holds also for the distribution of $D_{\mathrm{PB}} = 200$–400 km families in course of the time (age).

In this case, the synthetic production function of $D_{\mathrm{PB}} \gtrsim 100$ km families is *not* significantly affected by comminution. According to Bottke et al. (2005), most of $D > 10$ km fragments survive intact and a $D_{\mathrm{PB}} \gtrsim 100$ km family should be recognisable today. This is confirmed also by calculations with Boulder (see Figure 5, left column, 3rd row).

In order to improve the match between the synthetic and the observed production function, we can do the following: i) modify the scaling law; ii) account for a dynamical decay of the MB population. Using a substantially lower strength ($q_{\mathrm{fact}} = 5$ in Eq. (3), which is not likely, thought) one can obtain a synthetic production function which is *on average* consistent with the observations in the $D_{\mathrm{PB}} = 200$–400 km range.

Regarding the dynamical decay, Minton & Malhotra (2010) suggested that initially the MB was 3 times more populous than today while the decay timescale was very short — after 100 Myr of evolution the number of bodies is almost at the current level. In this brief period of time, about 50 % more families would be created, but all of them would be old, of course. For the remaining $\sim$ 3.9 Gyr, the above model (without any dynamical decay) is valid.

To conclude, it is possible – thought not very likely – that the observed families were produced by the collisional activity in the main belt alone. A dynamical decay of the MB population would create more families which are old, but technically speaking, this cannot be distinguished from the LHB scenario, which is to be discussed next.

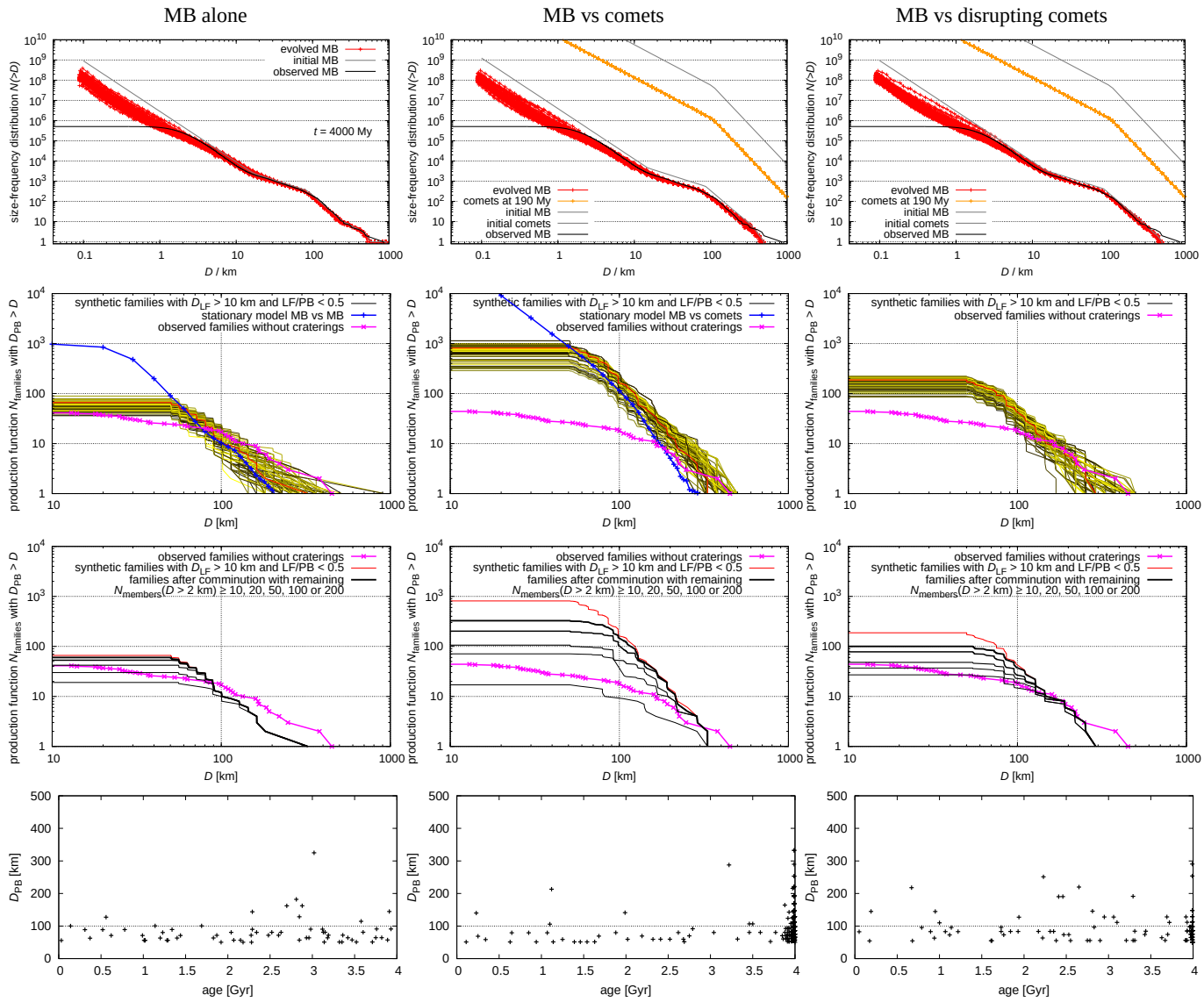

Fig. 5. Results of three different collisional models: main-belt alone which is discussed in Section 3 (left column), main-belt and comets from Section 4 (middle column), main-belt and disrupting comets from Section 7 (right column). We always show, in the 1st row: the initial and evolved size-frequency distributions of the main belt populations for 100 Boulder simulations; 2nd row: the resulting family production functions (in order to distinguish 100 lines we plot them using different colours ranging from black to yellow) and their comparison to the observations; 3rd row: the production function affected by comminution for a selected simulation; and 4th row: the distribution of synthetic families with $D_{\rm PB} \geq 50$ km in the (age, $D_{\rm PB}$) plot for a selected simulation, without comminution. Note that the positions of synthetic families in the 4th-row figures may differ significantly for a different Boulder simulation due to stochasticity and low-number statistics. Moreover, in the middle and right columns, many families were created during the LHB, so there are many overlapping crosses close to 4 Gyr.

4. Collisions between a "classical" cometary disk and the main belt

In this section, we are going to construct a collisional model and estimate an expected number of families created during the LHB due to collisions between cometary-disk bodies and main-belt asteroids. We start with a simple stationary model and we confirm the results using a more sophisticated Boulder code (Morbidelli et al. 2009).

Using the data from Vokrouhlický et al. (2008) for a "classical" cometary disk, we can estimate the intrinsic collisional probability and the collisional velocity between comets and asteroids. A typical time-dependent evolution of $P_{\rm i}$ and $V_{\rm imp}$ is shown in Figure 6. The probabilities increase at first, as the transneptunian cometary disk starts to decay, reaching up to 6×10^{-21} km^{-2} yr^{-1}, and after 100 Myr they decrease to zero. These results do *not* differ significantly from run to run.

4.1. Simple stationary model

In a stationary collisional model, we choose a SFD for the cometary disk, we assume a *current* population of the main belt, estimate the projectile size necessary to disrupt a given target according to (Bottke et al. 2005)

$$d_{\rm disrupt} = \left(2Q_D^\star / V_{\rm imp}^2\right)^{1/3} D_{\rm target}\,, \qquad (4)$$

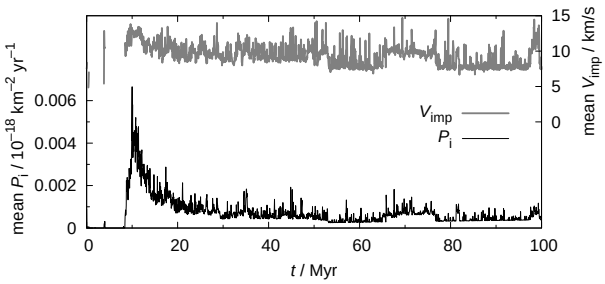

Fig. 6. The temporal evolution of the intrinsic collisional probability P_i (bottom) and mean collisional velocity V_imp (top) computed for collisions between cometary-disk bodies and the main-belt asteroids. The time $t = 0$ is arbitrary here; the sudden increase of P_i values corresponds to the beginning of the LHB.

where $Q_D^\star$ denotes the specific energy for disruption and dispersion of the target (Benz & Asphaug 1999), and finally calculate the number of events during the LHB as

$$n_\mathrm{events} = \frac{D_\mathrm{target}^2}{4}\, n_\mathrm{target} \int P_i(t)\, n_\mathrm{project}(t)\, \mathrm{d}t\,, \qquad (5)$$

where n_target and n_project are the number of targets (i.e. main belt asteroids) and the number of projectiles (comets), respectively. The actual number of bodies (27,000) in the dynamical simulation of Vokrouhlický et al. (2008) changes in course of time and it was scaled such that initially it was equal to the number of projectiles $N(>d_\mathrm{disrupt})$ inferred from the SFD of the disk. This is clearly a *lower limit* for the number of families created, since the main belt was definitely more populous in the past.

The average impact velocity is $V_\mathrm{imp} \simeq 10\,\mathrm{km/s}$ and we thus need the following projectile sizes to disrupt given target sizes:

D_target (km)	N_targets in the MB	$Q_D^\star$ (J/kg)	d_disrupt for $\frac{\rho_\mathrm{target}}{\rho_\mathrm{project}} = 3$ to 6 (km)
100	∼192	1×10^5	12.6 to 23
200	∼23	4×10^5	40.0 to 73

We try to use various SFD's for the cometary disk (i.e., with various differential slopes q_1 for $D > D_0$ and q_2 for $D < D_0$, the elbow diameter D_0 and total mass M_disk), including rather extreme cases (see Figure 7). The resulting numbers of LHB families are summarised in Table 6. Usually, we obtain several families with $D_\mathrm{PB} \simeq 200\,\mathrm{km}$ and about 100 families with $D_\mathrm{PB} \simeq 100\,\mathrm{km}$. This result is robust with respect to the slope q_2, because even very shallow SFD's should produce a lot of these families.[4] The only way to decrease the number of families significantly is to assume the elbow at a larger diameter $D_0 \simeq 150\,\mathrm{km}$.

It is thus no problem to explain the existence of approximately 5 *large* families with $D_\mathrm{PB} = 200$–$400\,\mathrm{km}$ which are indeed observed, since they can be readily produced during the LHB. On the other hand, the high number of $D_\mathrm{PB} \simeq 100\,\mathrm{km}$ families is clearly contradicting the observations, since we observe *almost no LHB families* of this size.

[4] The extreme case with $q_2 = 0$ is not likely at all, e.g. because of the continuous SFD of basins on Iapetus and Rhea, which exhibits only a mild depletion of $D \simeq 100\,\mathrm{km}$ size craters; see Kirchoff & Schenk (2010). On the other hand, Sheppard & Trujillo (2010) report an extremely shallow cumulative SFD of Neptune Trojans which is akin to low q_2.

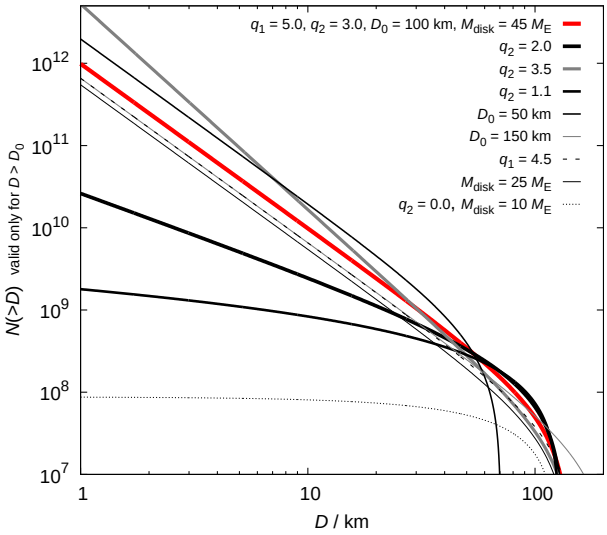

Fig. 7. Cumulative size-frequency distributions of the cometary disk which we tested in this work. All the parameters of our nominal choice are given in the top label; the other labels just report the parameters that changed relative to our nominal choice.

4.2. Constraints from (4) Vesta

The asteroid (4) Vesta presents a significant constraint for collisional models, being a differentiated body with preserved basaltic crust (Keil 2002) and a 500 km large basin on its surface (which is significantly younger than 4 Gyr; Marchi et al. 2012). It is highly unlikely that Vesta experienced a catastrophic disruption in the past and even large cratering events were limited. We thus have to check the number of collisions between one $D = 530\,\mathrm{km}$ target and $D \simeq 35\,\mathrm{km}$ projectiles which are capable to produce the basin and the Vesta family (Thomas et al. 1997). According to Table 6, the predicted number of such events does not exceed ∼ 2, so given the stochasticity of the results there is a significant chance that Vesta indeed experienced zero such impacts during the LHB.

4.3. Simulations with the Boulder code

In order to confirm results of the simple stationary model, we also perform simulations with the Boulder code. We modified the code to include a time-dependent collisional probabilities $P_\mathrm{i}(t)$ and impact velocities $V_\mathrm{imp}(t)$ of the cometary-disk population.

We start a simulation with a setup for the cometary disk resembling the nominal case from Table 6. The scaling law is described by Eq. (3), with the following parameters (the first set corresponds to basaltic material at 5 km/s, the second one to water ice, Benz & Asphaug 1999):

	ρ (g/cm^3)	Q_0 (erg/g)	a	B (erg/g)	b	q_fact
asteroids	3.0	7×10^7	−0.45	2.1	1.19	1.0
comets	1.0	1.6×10^7	−0.39	1.2	1.26	3.0

The intrinsic probabilities $P_\mathrm{i} = 3.1 \times 10^{-18}\,\mathrm{km^{-2}\,yr^{-1}}$ and velocities $V_\mathrm{imp} = 5.28\,\mathrm{km/s}$ for the MB vs MB collisions were again taken from the work of Dahlgren (1998). We do not account for comet–comet collisions since their evolution is dominated by the dynamical decay.

Table 6. Results of a stationary collisional model between the cometary disk and the main belt. The parameters characterise the SFD of the disk: q_1, q_2 are differential slopes for the diameters larger/smaller than the elbow diameter D_0, $M_{\rm disk}$ denotes the total mass of the disk, and $n_{\rm events}$ is the resulting number of families created during the LHB for a given parent body size $D_{\rm PB}$. The ranges of $n_{\rm events}$ are due to variable density ratios $\rho_{\rm target}/\rho_{\rm project}$ = 1 to 3/1.

q_1	q_2	D_0 (km)	$M_{\rm disk}$ ($M_\oplus$)	$n_{\rm events}$ for $D_{\rm PB} \geq 100$ km	$D_{\rm PB} \geq 200$ km	Vesta craterings	notes
5.0	3.0	100	45	115–55	4.9–2.1	2.0	nominal case
5.0	2.0	100	45	35–23	4.0–2.2	1.1	shallow SFD
5.0	3.5	100	45	174–70	4.3–1.6	1.8	steep SFD
5.0	1.1	100	45	14–12	3.1–2.1	1.1	extremely shallow SFD
4.5	3.0	100	45	77–37	3.3–1.5	1.3	lower q_1
5.0	3.0	50	45	225–104	7.2–1.7	3.2	smaller turn-off
5.0	3.0	100	25	64–40	2.7–1.5	1.1	lower $M_{\rm disk}$
5.0	3.0	100	17	34	1.2	1.9	$\rho_{\rm comets}$ = 500 kg/m^3
5.0	3.0	150	45	77–23	3.4–0.95	0.74	larger turn-off
5.0	0.0	100	10	1.5–1.4	0.5–0.4	0.16	worst case (zero q_2 and low $M_{\rm disk}$)

The resulting size-frequency distributions of 100 independent simulations with different random seeds are shown in Figure 5 (middle column). The number of LHB families (approximately 10 with $D_{\rm PB} \simeq 200$ km and 200 with $D_{\rm PB} \simeq 100$ km) is even *larger* compared to the stationary model, as expected, because we have to start with a larger main belt to get a good fit of the currently observed MB after 4 Gyr of collisional evolution.

To conclude, the stationary model and the Boulder code give results which are compatible with each other, but clearly contradict the observed production function of families. In particular, they predict far too many families with $D = 100$ km parent bodies. At first sight, this may be interpreted as a proof that there was no cometary LHB on the asteroids. Before jumping at this conclusion, however, one has to investigate whether there are biases against the identification of $D_{\rm PB} = 100$ km families. In Sections 5–9 we discuss several mechanisms which all contribute, at some level, to reducing the number of observable $D_{\rm PB} = 100$ km families over time. They are addressed in order of relevance, from the least to the most effective.

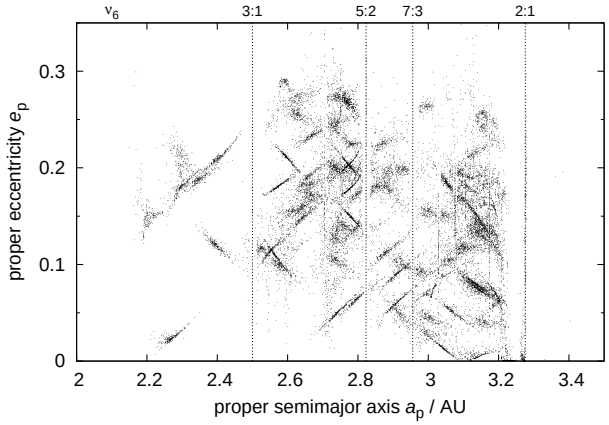

Fig. 8. The proper semimajor axis $a_{\rm p}$ vs the proper eccentricity $e_{\rm p}$ for 100 synthetic families created in the main belt. It is the *initial* state, shortly after disruption events. We assume the size-frequency distribution of bodies in each synthetic family similar to that of the Koronis family (down to $D \simeq 2$ km).

5. Families overlap

Because the number of expected $D_{\rm PB} \geq 100$ km LHB families is very high (of the order 100) we now want to verify if these families can *overlap* in such a way that they cannot be distinguished from each other and from the background. We thus take 192 main-belt bodies with $D \geq 100$ km and select randomly 100 of them which will disrupt. For every one we create an artificial family with 10^2 members, assume a size-dependent ejection velocity $V \propto 1/D$ (with $V = 50$ m/s for $D = 5$ km) and the size distribution resembling that of the Koronis family. We then calculate proper elements ($a_{\rm p}, e_{\rm p}, \sin I_{\rm p}$) for all bodies.

According to the resulting Figure 8 the answer to the question is simple: the families do *not* overlap sufficiently and they cannot be hidden that way. Moreover, if we take only bigger bodies ($D > 10$ km) these would be clustered even more tightly. The same is true for proper inclinations, which are usually more clustered than eccentricities, so families could be more easily recognised.

6. Dispersion of families by the Yarkovsky drift

In this section, we model long-term evolution of synthetic families driven by the Yarkovsky effect and chaotic diffusion. For *one* synthetic family located in the outer belt, we perform a full N-body integration with the SWIFT package (Levison & Duncan 1994), which includes also an implementation of the Yarkovsky/YORP effect (Brož 2006) and 2nd order integrator by Laskar & Robutel (2001). We include 4 giant planets in this simulation. In order to speed-up the integration, we use 10 times smaller sizes of the test particles and thus 10 times shorter time span (400 Myr instead of 4 Gyr). The selected time step is $\Delta t = 91$ d. We compute proper elements, namely their differences $\Delta a_{\rm p}, \Delta e_{\rm p}, \Delta \sin I_{\rm p}$ between the initial and final positions.

Then we use a simple *Monte-Carlo* approach for the whole set of 100 synthetic families — we assign a suitable drift $\Delta a_{\rm p}(D)$ in semimajor axis, and also drifts in eccentricity $\Delta e_{\rm p}$ and inclination $\Delta \sin I_{\rm p}$ to each member of 100 families, respecting asteroid sizes, of course. This way we account for the Yarkovsky semimajor axis drift and also for interactions with mean-motion and secular resonances. Such Monte-Carlo method tends to smear all structures, so we can regard our results as the *upper limits* for dispersion of families.

While the eccentricities of small asteroids (down to $D \simeq 2$ km) seem to be dispersed enough to hide the families, there are still some persistent structures in inclinations which would be observable today. Moreover, large asteroids ($D \geq 10$ km) seem to be clustered even after 4 Gyr, so that more than 50 % of families can be easily recognised against the background (see Figure 9). We thus can conclude that it is *not* possible to disperse the families by the Yarkovsky effect alone.

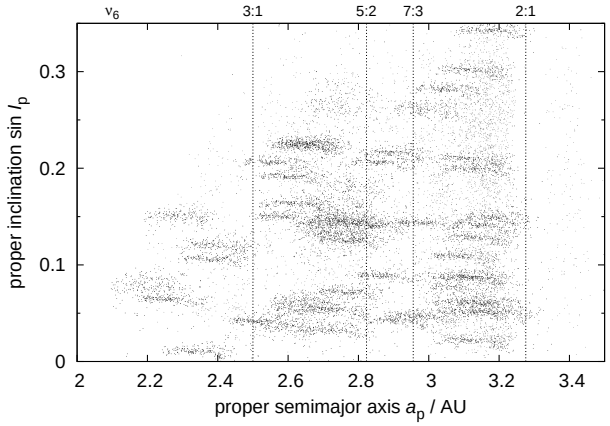

Fig. 9. The proper semimajor axis a_p vs the proper inclination $\sin I_p$ for 100 synthetic asteroid families (black dots), *evolved* over 4 Gyr using a Monte-Carlo model. The assumed SFD's correspond to the Koronis family, but we show only $D > 10$ km bodies here. We also include $D > 10$ km background asteroids (gray dots) for comparison.

7. Reduced physical lifetime of comets in the MB crossing zone

In order to illustrate the effects that the physical disruption of comets (due to volatile pressure build-up, amorphous/crystalline phase transitions, spin-up by jets etc.) can have on the collisional evolution of the asteroid belt, we adopt here a simplistic assumption: we consider that no comet disrupt beyond 1.5 AU, whereas all comets disrupt the first time that they penetrate inside 1.5 AU. Both conditions are clearly not true in reality: some comets are observed to blow up beyond 1.5 AU and others are seen to survive on Earth crossing orbit. Thus we adopt our disruption law just as an example of a drastic reduction of the number of comets with small perihelion distance, as required to explain the absence of evidence for a cometary bombardment on the Moon.

We then removed all those objects from output of comet evolution during the LHB that had a passage within 1.5 AU from the Sun, from the time of their first passage below this threshold. We then re-computed the mean intrinsic collision probability of a comet with the asteroid belt. The result is a factor ∼3 smaller than when no physical disruption of comets is taken into account as in Fig. 6. The mean impact velocity with asteroids also decreases, from 12 km/s to 8 km/s.

The resulting number of asteroid disruption events is thus decreased by a factor ∼4.5 which can be also seen on the production function shown in Figure 5 (right column). The production of families with $D_{\rm PB} = 200$–400 km is consistent with observations while the number of $D_{\rm PB} \simeq 100$ km families is reduced to 30–70, but is still too high, by a factor 2–3. More importantly, the slope of the production function remains steeper than that of the observed function. Thus, our conclusion is that physical disruptions of comets *cannot* explain alone the observation, but may be an important factor to keep into account to reconcile the model with the data.

8. Perturbation of families by migrating planets (a jumping-Jupiter scenario)

In principle, families created during the LHB may be perturbed by still-migrating planets. It is an open question what was the exact orbital evolution of planets at that time. Nevertheless, a plausible scenario called a "jumping Jupiter" was presented by Morbidelli et al. (2010). It explains major features of the main belt (namely the paucity of high-inclination asteroids above the ν_6 secular resonance), it is consistent with amplitudes of the secular frequencies of both giant and terrestrial planets and also with other features of the solar system. In this work, we thus investigate this particular migration scenario.

We use the data from Morbidelli et al. (2010) for the orbital evolution of giant planets. We then employ a modified SWIFT integrator, which reads orbital elements for planets from an input file and calculates only the evolution of test particles. Four synthetic families located in the inner/middle/outer belt were integrated. We start the evolution of planets at various times, ranging from t_0 to $(t_0 + 4\,\mathrm{Myr})$ and we stop the integration at $(t_0 + 4\,\mathrm{My})$, in order to test the perturbation on families created in different phases of migration. Finally, we calculate proper elements of asteroids when the planets do not migrate anymore. (We also have to move planets smoothly to their exact current orbital positions.)

The results are shown in Figure 10. While the proper eccentricities seem to be sufficiently perturbed and families are dispersed even when created at late phases of migration, the proper inclinations are not very dispersed, except for families in the outer asteroid belt that formed at the very beginning of the giant planet instability (which may be unlikely, as there must be a delay between the onset of planet instability and the beginning of the cometary flux through the asteroid belt). In most cases, the LHB families could still be identified as clumps in semi-major axis vs inclination space. We do not see any of such $(a_{\rm p}, \sin I_{\rm p})$-clumps, dispersed in eccentricity, in the asteroid belt.[5]

The conclusion is clear: it is *not* possible to destroy low-e and low-I families by perturbations arising from giant-planet migration, at least in the case of the "jumping-Jupiter" scenario.[6]

9. Collisional comminution of asteroid families

We already mentioned that the comminution is *not* sufficient to destroy a $D_{\rm PB} = 100$ km family *in the current environment* of the main belt (Bottke et al. 2005).

However, the situation in case of the LHB scenario is different. Both the large population of comets and several-times larger main belt, which has to withstand the cometary bombardment, contribute to the enhanced comminution of the LHB families. To estimate the amount of comminution, we perform the following calculations: i) for a selected collisional simulation – whose production function is close to the average one – we record the SFD's of all synthetic families created in course of time ii) for each synthetic family, we restart the simulation from the time t_0 when the family was crated till 4 Gyr and save the final SFD, i.e. after the comminution. The results are shown in Figure 11.

It is now important to discuss criteria, which enable us to decide if the comminutioned synthetic family would be indeed observable or not. We use the following set of conditions: $D_{\rm PB} \geq 50$ km, $D_{\rm LF} \geq 10$ km (largest *fragment* is the 1st or the 2nd largest body, where the SFD becomes steep), LR/PB < 0.5 (i.e. a catastrophic disruption). Furthermore, we define $N_{\rm members}$ as

[5] Note that high-inclination families would be dispersed much more due to the Kozai mechanism, because eccentricities, which are sufficiently perturbed, exhibit oscillations coupled with inclinations.

[6] The today-non-existent families around (107) Camilla and (121) Hermione — inferred from the existence of their satellites — cannot be destroyed in the jumping-Jupiter scenario, unless the families were actually *pre*-LHB and experienced the jump.

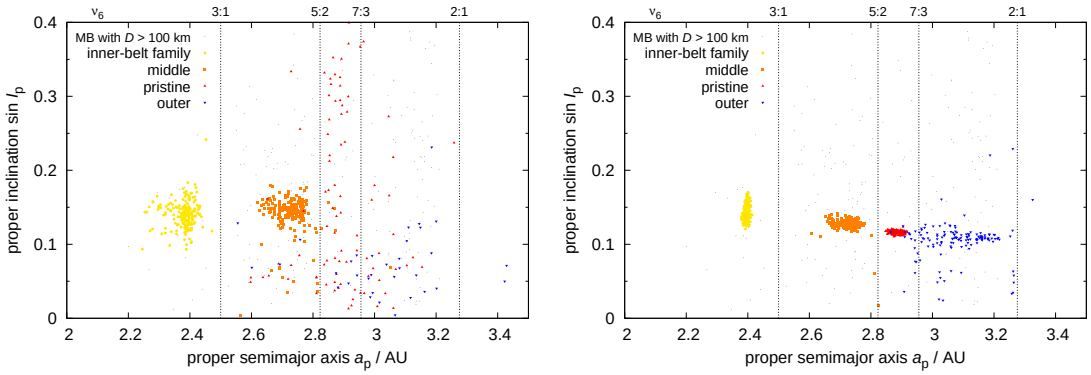

Fig. 10. The proper semimajor axis vs the proper inclination for four synthetic families (distinguished by symbols) as perturbed by giant-planet migration. Left panel: the case when families were evolved over the "jump" due to the encounter between Jupiter and Neptune. Right panel: the families created just after the jump and perturbed only by later phases of migration.

the number of the *remaining* family members larger than observational limit $D_{\rm limit} \simeq 2$ km and use a condition $N_{\rm members} \geq 10$. The latter number depends on the position of the family within the main belt, thought. In the favourable "almost-empty" zone (between $a_{\rm p} = 2.825$ and 2.955 AU) $N_{\rm members} \geq 10$ may be valid, but in a populated part of the MB one would need $N_{\rm members} \gtrsim 100$ to detect the family. The size-distributions of synthetic families selected this way resemble the observed SFD's of the main-belt families.

According to Figure 5 (3rd row), where we can see the production functions after comminution for increasing values of $N_{\rm members}$, families with $D_{\rm PB} = 200$–400 km remain *more prominent* than $D_{\rm PB} \simeq 100$ km families simply because they contain much more members with $D > 10$ km which survive intact. Our conclusion is thus that comminution may explain the paucity of the observed $D_{\rm PB} \simeq 100$ km families.

10. "Pristine zone" between the 5:2 and 7:3 resonances

Let us now focus on the zone between the 5:2 and 7:3 mean-motion resonances, with $a_{\rm p} = 2.825$ to 2.955 AU, which is not so populated as the surrounding regions of the main belt (see Figure 1). This is a unique situation, because both bounding resonances are strong enough to prevent any asteroids from outside to enter this zone due the Yarkovsky semimajor axis drift. Any family formation event in the surroundings has only a minor influence on this narrow region. It thus can be called "pristine zone" because it may resemble the belt *prior* to creation of big asteroid families.

We identified 9 previously unknown small families which are visible on the $(e_{\rm p}, \sin I_{\rm p})$ plot (see Figure 12). They are confirmed by the SDSS colours and WISE albedos too. Nevertheless, there is *only one* big and old family in this zone ($D_{\rm PB} \geq 100$ km), i.e. Koronis.

The fact that at most one LHB family (Koronis) is observed in the "pristine zone" can give us a simple probabilistic estimate for the *maximum* number of disruptions during the LHB. Let us take the 192 existing main-belt bodies which have $D \geq 100$ km and select randomly 100 of them which will disrupt. We repeat this selection 1000 times and always count the number of families in the pristine zone. The resulting histogram is shown in Figure 13. As we can see, there is very low (<0.001) probability that the number of families in the pristine zone is zero or one. On average we get 8 families there. It seems that either the number of disruptions should be substantially lower than 100 or we expect to find at least some "remnants" of the LHB families here.

It is interesting that the SFD of an old comminutioned family is *very flat* in the range $D = 1$ to 10 km (see Figure 11) — similar to those of some of the "less-certain" observed families! We may speculate that the families like (918) Itha, (5567) Durisen, (12573) 1999 NJ_{53} or (15454) 1998 YB_3 (all from the pristine zone) are actually remnants of *larger and older* families, even though they are denoted as young. May be, the age estimate based on the $(a_{\rm p}, H)$ analysis is incorrect since small bodies were destroyed by comminution and spread by the Yarkovsky effect too far away from the largest remnant, so they can be no more identified with the family.

Finally, we have to ask an important question: how an old/comminutioned family with $D_{\rm PB} \simeq 100$ km looks like in the proper-element space? To this aim, we created a synthetic family in the "pristine zone", we assumed the family has $N_{\rm members} \simeq 100$ larger than $D_{\rm limit} \simeq 2$ km and the SFD is already flat in the $D = 1$ to 10 km range. We evolved the asteroids up to 4 Gyr due to the Yarkovsky effect and gravitational perturbations, using the N-body integrator as in Section 6. Most of the $D \simeq 2$ km bodies were lost in course of the dynamical evolution, of course. The resulting family is shown in Figure 14. We can also imagine that this family is placed in the pristine zone among other observed families, to get a feeling if it is easily observable or not (refer to Figure 12).

It is clear that such family is *hardly observable* even in the almost-empty zone of the main belt! Conclusion is that the comminution (as given by the Boulder code) *can explain* the paucity of $D_{\rm PB} \simeq 100$ km LHB families, since we can hardly distinguish old families from the background.

11. Conclusions

In this paper we investigated the cometary bombardment of the asteroid belt at the time of the LHB, in the framework of the Nice model.

There are many evidences for a high cometary flux through the giant planets region, but no strong evidence for a cometary bombardment on the Moon. This suggests that many comets disrupted on their way to the inner solar system. By investigating the collisional evolution of the asteroid belt and comparing the results to the collection of actual collisional families, our aim was to constrain whether or not the asteroid belt experienced an intense cometary bombardment at the time of the LHB and, if possible, constrain the intensity of said bombardment.

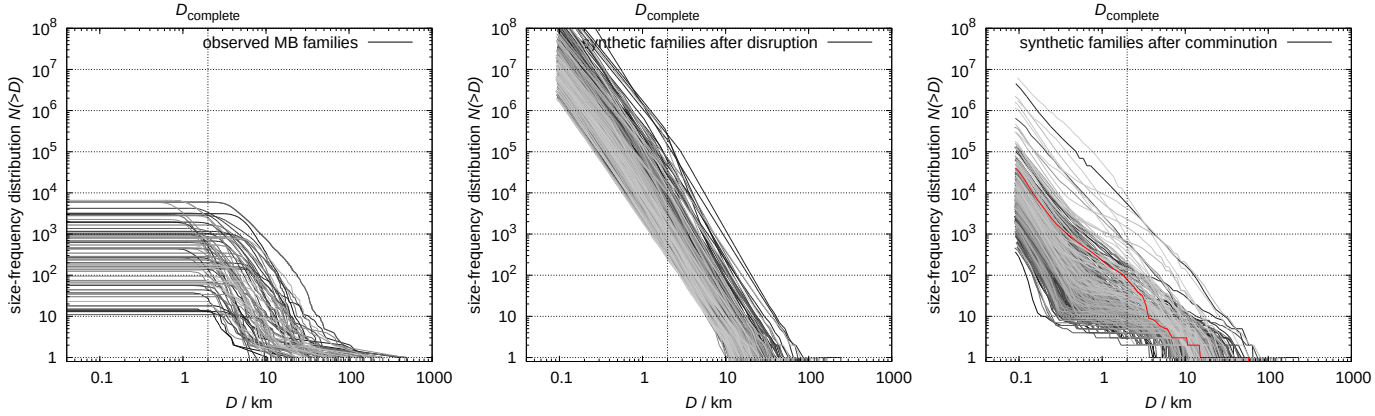

Fig. 11. Left panel: the size-frequency distributions of the observed asteroid families. Middle panel: SFD's of 378 distinct synthetic families created during one of the collisional simulations of the MB and comets. Note that initially, all synthetic SFD's are very steep, in agreement with SPH simulations (Durda et al. 2007). We plot only the SFD's which fulfil the following criteria: $D_{\rm PB} \geq 50$ km, $D_{\rm LF} \geq 10$ km, LR/PB < 0.5 (i.e. catastrophic disruptions). Right panel: the evolved SFD's after comminution. Only a minority of families is observable now, since the number of remaining members larger that observational limit $D_{\rm limit} \simeq 2$ km is often much smaller than 100. The SFD which we use for the simulation in Section 10 is denoted by red colour.

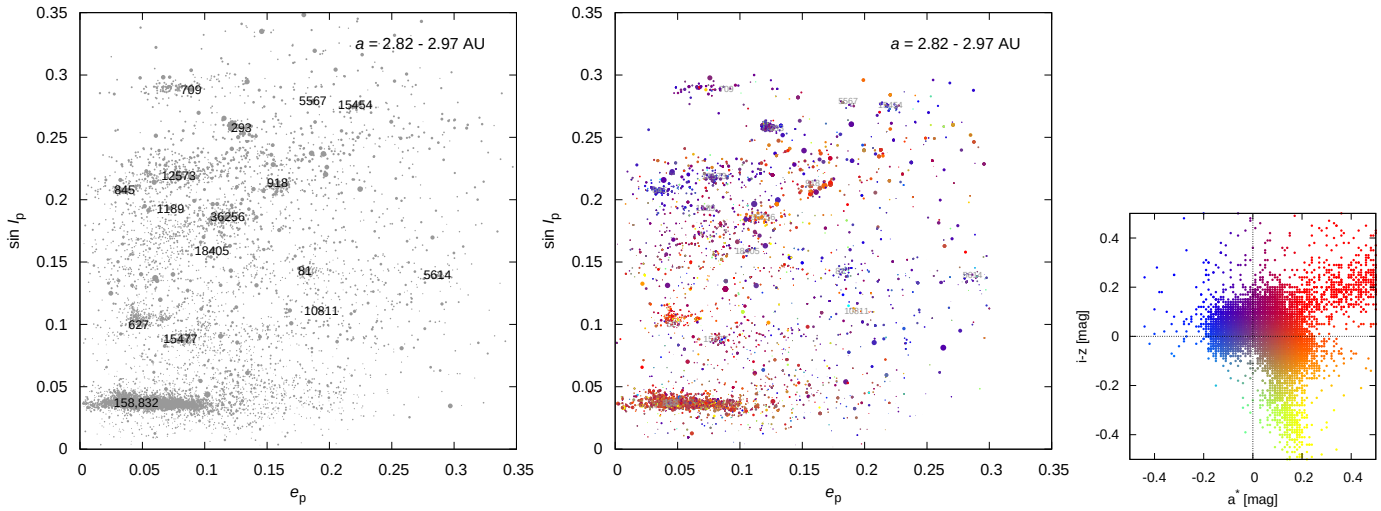

Fig. 12. The "pristine zone" of the main belt ($a_{\rm p} = 2.825$ to 2.955 AU) displayed on the proper eccentricity $e_{\rm p}$ vs proper inclination $\sin I_{\rm p}$ plot. Left panel: the sizes of symbols correspond to the sizes of asteroids, the families are denoted by designations. Right panel: a subset of bodies for which SDSS data are available; the colours of symbols correspond to the SDSS colour indices a^* and $i - z$ (Parker et al. 2008).

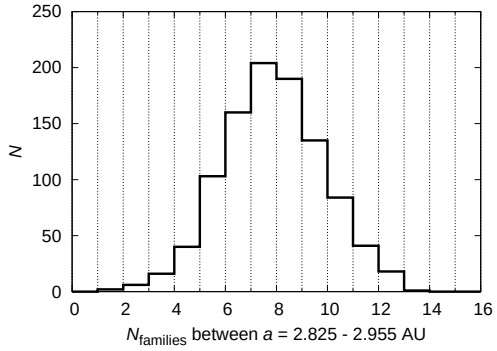

Fig. 13. The histogram for the expected number of LHB families located in the "pristine zone" of the main belt.

Observations suggest that the number of collisional families is a very shallow function of parent-body size (that we call in this paper the "production function"). We show that the collisional activity of the asteroid belt as a closed system, i.e. without any external cometary bombardment, in general does not produce such a shallow production function. Moreover, the number of families with parent bodies larger than 200 km in diameter is in general too small compared to the observations. However, there is a lot of stochasticity in the collisional evolution of the asteroid belt and about 5 % of our simulations actually fit the observational constraints (shallowness of the production function and number of large families) quite well. Thus, in principle, there is no need for a bombardment due to external agents (i.e. the comets) to explain the asteroid family collection, provided that the real collisional evolution of the main belt was a "lucky" one and not the "average" one.

If one accounts for the bombardment provided by the comets crossing the main belt at the LHB time, predicted by the Nice model, one can easily justify the number of observed families with parent body larger than 200 km. However, the resulting production function is steep, and the number of families produced by parent bodies of 100 km is almost an order of magnitude too large.

We have investigated several processes that may decimate the number of families identifiable today with 100 km parent

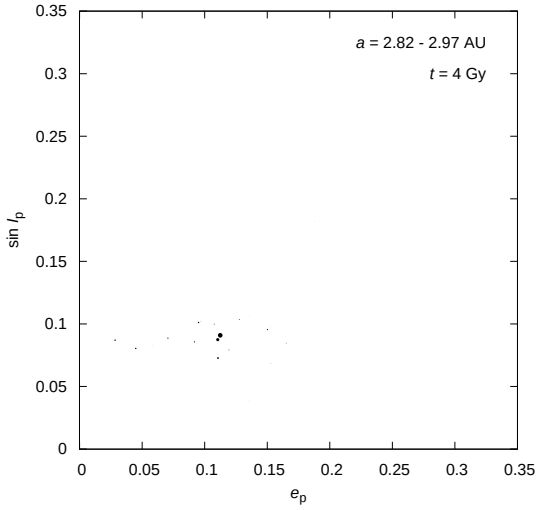

Fig. 14. The proper eccentricity vs proper inclination of one synthetic old/comminutioned family evolved dynamically over 4 Gyr. Only a few family members ($N \simeq 10^1$) remained from the original number of $N(D \geq 2\,\mathrm{km}) \simeq 10^2$. The scales are the same as in Figure 12, so we can compare it easily to the "pristine zone".

bodies, without affecting considerably the survival of families formed from larger parent bodies. Of all these processes, the collisional comminution of the families and their dispersal by the Yarkovsky effect are the most effective ones. With the help of the physical disruption of comets due to activity, which can reduce the effective cometary flux through the belt by a factor up to 5, the resulting distribution of families can be consistent with observations.

We can also think of two "alternative" explanations: i) physical lifetime of comets was strongly size-dependent so that smaller bodies disrupt easily compared to bigger ones; ii) high-velocity collisions between hard targets (asteroids) and *very* weak projectiles (comets) may result in different outcomes than in low-velocity regimes explored so far. Our work thus may serve as a motivation for further SPH simulations.

Our results are consequently relatively weak. We cannot demonstrate that a LHB occurred on asteroids due to cometary bombardment. We cannot constrain the maximal cometary flux relative to that predicted in the Nice model. However, we show that the family distribution in the asteroid belt is *not in contradiction* with a cometary LHB.

Acknowledgements

The work of MB and DV has been supported by the Grant Agency of the Czech Republic (grants no. 205/08/P196, 205/08/0064 and 13-09208S) and the Research Program MSM0021620860 of the Czech Ministry of Education. We also acknowledge the usage of computers of the Observatory and Planetarium in Hradec Králové.

References

Benz, W., & Asphaug, E. 1999, Icarus, 142, 5
Bogard, D.D. 1995, Meteoritics, 30, 244
Bogard, D.D. 2011, Chemie der Erde – Geochemistry, 71, 207
Bottke, W.F., Vokrouhlický, D., Brož, M., Nesvorný, D., & Morbidelli, A. 2001, Science, 294, 1693
Bottke, W.F., Durda, D.D., Nesvorný, D., et al. 2005, Icarus, 175, 111
Bottke, W.F., Levison, H.F., Nesvorný, D., & Dones, L. 2007, Icarus, 190, 203
Bottke, W.F., Vokrouhlický, D., & Nesvorný, D. 2007, Nature, 449, 48
Bottke, W.F., Nesvorný, D., Vokrouhlický, D., & Morbidelli, A. 2010, AJ, 139, 994
Bottke, W.F., Vokrouhlický D., Minton, D., et al. 2012, Nature, in press
Brož, M. 2006, PhD thesis, Charles Univ.
Brož, M., Vokrouhlický, D., Morbidelli, A., Nesvorný. D., & Bottke, W.F. 2011, MNRAS, 414, 2716
Carruba, V. 2009, MNRAS, 398, 1512
Carruba, V. 2010, MNRAS, 408, 580
Chapman, C.R., Cohen, B.A., Grinspoon, D.H. 2007, Icarus, 189, 233
Charnoz, S., Morbidelli, A., Dones, L., & Salmon, J. 2009, Icarus, 199, 413
Cohen, B.A., Swindle, T.D., & Kring, D.A. 2000, Science, 290, 1754
Dahlgren, M. 1998, A&A, 336, 1056
Durda, D.D., Bottke, W.F., Nesvorný, D., et al. 2007, 186, 498
Foglia, S., & Masi, G., 2004, Minor Planet Bull., 31, 100
Gil-Hutton, R. 2006, Icarus, 183, 83
Gomes, R., Levison, H.F., Tsiganis, K., & Morbidelli, A. 2005, Nature, 435, 466
Hartmann, W.K., Ryder, G., Dones, L., & Grinspoon, D. 2000, in Origin of the Earth and Moon, ed. R.M. Canup, K. Righter, Tucson: University of Arizona Press, p. 493
Hartmann, W.K., Quantin, C., & Mangold, N. 2007, Icarus, 186, 11
Keil, K. 2002, in Asteroids III, ed. W.F. Bottke Jr., A. Cellino, P. Paolicchi, R.P. Binzel, Tucson: University of Arizona Press, p. 573
Kirchoff, M.R., & Schenk, P. 2010, Icarus, 206, 485
Knežević, Z., & Milani, A. 2003, A&A, 403, 1165
Koeberl, C. 2004, Geochimica et Cosmochimica Acta, 68, 931
Kring, D.A., & Cohen, B.A. 2002, J. Geophys. Res., 107, 41
Laskar, J., & Robutel, P. 2001, Celest. Mech. Dyn. Astron., 80, 39
Levison, H.F., & Duncan, M. 1994, Icarus, 108, 18
Levison, H.F., Bottke, W.F., Gounelle, M., et al. 2009, Nature, 460, 364
Margot, J.-L., & Rojo, P. 2007, BAAS, 39, 1608
Marzari, F., Farinella, P., & Davis, D.R. 1999, Icarus, 142, 63
Masiero, J.P., Mainzer A.K., Grav, T., et al. 2011, ApJ, 741, 68
Michel, P., Tanga, P., Benz, & W., Richardson, D.C. 2002, Icarus, 160, 10
Michel, P., Jutzi, M., Richardson, D.C., & Benz, W. 2011, Icarus, 211, 535
Minton, D.A., & Malhotra, R. 2009, Nature, 457, 1109
Minton, D.A., & Malhotra, R. 2010, Icarus, 207, 744
Morbidelli, A. 2010, Comptes Rendus Physique, 11, 651
Morbidelli, A., Tsiganis, K., Crida, A., Levison, H.F., & Gomes, R. 2007, AJ, 134, 1790
Morbidelli, A., Levison, H.F., Bottke, W.F., Dones, L., & Nesvorný, D. 2009, Icarus, 202, 310
Morbidelli, A., Brasser, R., Gomes, R., Levison, H.F., & Tsiganis, K. 2010, AJ, 140, 1391
Morbidelli, A., Marchi, S., & Bottke, W.F. 2012, LPI Cont. 1649, 53
Molnar, L.A., & Haegert, M.J. 2009, BAAS, 41, 2705
Nesvorný, D. 2010, EAR-A-VARGBDET-5-NESVORNYFAM-V1.0, NASA Planetary Data System
Nesvorný, D., & Vokrouhlický, D. 2006, AJ, 132, 1950
Nesvorný, D., Morbidelli, A., Vokrouhlický, D., Bottke, W.F., & Brož, M. 2002, Icarus, 157, 155
Nesvorný, D., Jedicke, R., Whiteley, R.J., & Ivezić, Ž. 2005, Icarus, 173, 132
Nesvorný, D., Vokrouhlický, D., & Morbidelli, A. 2007, AJ, 133, 1962
Nesvorný, D., Vokrouhlický, D., Morbidelli, A., & Bottke, W.F. 2009, Icarus, 200, 698
Neukum, G., Ivanov, B.A., & Hartmann, W.K. 2001, Space Sci. Rev., 96, 55
Norman, M.D., & Nemchin, A.A. 2012, LPI Cont., 1659, 1368
Novaković, B. 2010, MNRAS, 407, 1477
Novaković, B., Tsiganis, K., & Knežević, Z. 2010, Celest. Mech. Dyn. Astron., 107, 35
Novaković, B., Cellino, A., & Knežević, Z. 2011, Icarus, 216, 69
Parker, A., Ivezić, Ž., Jurić, M, et al. 2008, Icarus, 198, 138
Ryder, G., Koeberl, C., & Mojzsis, S.J. 2000, in Origin of the Earth and Moon, ed. R.M. Canup, K. Righter, Tucson: University of Arizona Press, p. 475
Sheppard, S.S, & Trujillo, C.A. 2010, ApJL, 723, L233
Strom, R.G., Malhotra, R., Ito, T., Yoshida, F., & Kring, D.A. 2005, Science, 309, 1847.
Swindle, T.D., Isachsen, C.E., Weirich, J.R., & Kring, D.A. 2009, Meteor. Planet. Sci., 44, 747
Tagle, R. 2005, LPI Cont., 36, 2008
Tedesco, E.F., Noah, P.V., Noah, M., & Price, S.D. 2002, AJ, 123, 1056
Tera, F., Papanastassiou, D.A., & Wasserburg, G.J. 1974, Earth & Planet. Sci. Let., 22, 1
Tsiganis K., Gomes, R., Morbidelli, A., & Levison, H.F. 2005, Nature, 435, 459
Thomas, P.C., Binzel, R.P., Gaffey, M.J., et al. 1997, Science, 277, 1492
Vokrouhlický, D., & Nesvorný, D. 2011, AJ, 142, 26
Vokrouhlický, D., Brož, M., Bottke, W.F., Nesvorný, D., & Morbidelli, A. 2006, Icarus, 182, 118
Vokrouhlický, D., Nesvorný, D., & Levison, H.F. 2008, AJ, 136, 1463

Vokrouhlický, D., Nesvorný, D., Bottke, W.F., & Morbidelli, A. 2010, AJ, 139, 2148
Warner, B.D., Harris, A.W., Vokrouhlický, D., Nesvorný, D., & Bottke, W.F. 2009, Icarus, 204, 172
Weidenschilling, S.J. 2000, Space Sci. Rev., 92, 295
Zappalà, V., Bendjoya, Ph., Cellino, A., Farinella, P., & Froeschlé, C. 1995, Icarus, 116, 291

Table 1. A list of asteroid families and their physical parameters. There are the following columns: $v_{\rm cutoff}$ is the selected cut–off velocity for the hierarchical clustering, N the corresponding number of family members, p_V the adopted value of the geometric albedo for family members which do not have measured diameters (from Tedesco et al. 2002 or Masiero et al. 2011, a letter 'w' indicates it was necessary to use the WISE data to obtain median/mean albedo), taxonomic classification (according to the Sloan DSS MOC 4 colours, Parker et al. 2008), $D_{\rm PB}$ parent body size, an additional 'c' letter indicates that we prolonged the SFD slope down to zero D (a typical uncertainty is 10 %), $D_{\rm Durda}$ PB size inferred from SPH simulations (Durda et al. 2007), an exclamation mark denotes a significant mismatch with $D_{\rm PB}$, LR/PB the ratio of the volumes of the largest remnant to the parent body (an uncertainty corresponds to the last figure, a range is given if both $D_{\rm PB}$ and $D_{\rm Durda}$ are known), $v_{\rm esc}$ the escape velocity, q_1 the slope of the SFD for larger D, q_2 the slope for smaller D (a typical uncertainty of the slopes is 0.2, if not indicated otherwise), dynamical age including its uncertainty.

designation		$v_{\rm cutoff}$ m/s	N	p_V	tax.	$D_{\rm PB}$ km	$D_{\rm Durda}$ km	LR/PB	$v_{\rm esc}$ m/s	q_1	q_2	age Gyr	notes, references
3	Juno	50	449	0.250	S	233	?	0.999	139	−4.9	−3.2	<0.7	cratering, Nesvorný et al. (2005)
4	Vesta	60	11169	0.351w	V	530	425!	0.995	314	−4.5	−2.9	1.0 ± 0.25	cratering, Marchi et al. (2012)
8	Flora	60	5284	0.304w	S	150c	160	0.81-0.68	88	−3.4	−2.9	1.0 ± 0.5	cut by ν_6 resonance, LL chondrites
10	Hygiea	70	3122	0.055	C,B	410	442	0.976-0.78	243	−4.2	−3.2	2.0 ± 1.0	LHB? cratering
15	Eunomia	50	2867	0.187	S	259	292	0.958-0.66	153	−5.6	−2.3	2.5 ± 0.5	LHB? Michel et al. (2002)
20	Massalia	40	2980	0.215	S	146	144	0.995	86	−5.0	−3.0	0.3 ± 0.1	
24	Themis	70	3581	0.066	C	268c	380-430!	0.43-0.09	158	−2.7	−2.4	2.5 ± 1.0	LHB?
44	Nysa (Polana)	60	9957	0.278w	S	81c	?	0.65	48	−6.9	−2.6(0.5)	<1.5	overlaps with the Polana family
46	Hestia	65	95	0.053	S	124	153	0.992-0.53	74	−3.3	−2.0	<0.2	cratering, close to J3/1 resonance
87	Sylvia	110	71	0.045	C/X	261	272	0.994-0.88	154	−5.2	−2.4	1.0-3.8	LHB? cratering, Vokrouhlický et al. (2010)
128	Nemesis	60	654	0.052	C	189	197	0.987-0.87	112	−3.4	−3.3	0.2 ± 0.1	
137	Meliboea	95	199	0.054	C	174c	240-290!	0.59-0.20	102	−1.9	−1.8	<3.0	old?
142	Polana (Nysa)	60	3443	0.055w	C	75	?	0.42	45	−7.0	−3.6	<1.5	overlaps with Nysa
145	Adeona	50	1161	0.065	C	171c	185	0.69-0.54	101	−5.2	−2.8	0.7 ± 0.5	cut by J5/2 resonance
158	Koronis	50	4225	0.147	S	122c	170-180	0.024-0.009	68	−3.6(0.3)	−2.3	2.5 ± 1.0	LHB?
163	Erigone	60	1059	0.056	C/X	79	114	0.79-0.26	46	?	−3.6	0.3 ± 0.2	
170	Maria	80	3094	0.249w	S	107c	120-130	0.070-0.048	63	−2.5(0.3)	−2.8	3.0 ± 1.0	LHB?
221	Eos	50	5976	0.130	K	208c	381!	0.13-0.020	123	−3.5	−2.1	1.3 ± 0.2	
283	Emma	75	345	0.050	-	152	185	0.92-0.51	90	?	−3.2	<1.0	satellite
293	Brasilia	60	282	0.175w	C/X	34	?	0.020	20	−1.4(0.5)	−3.7	0.05 ± 0.04	(293) is interloper
363	Padua (Lydia)	50	596	0.097	C/X	76	106	0.045-0.017	45	−1.8	−3.0	0.3 ± 0.2	
396	Aeolia	20	124	0.171	C/X	35	39	0.966-0.70	20	?	−4.3	<0.1	cratering
410	Chloris	90	259	0.057	C	126c	154	0.952-0.52	74	?	−2.1	0.7 ± 0.4	
490	Veritas	-	-	-	C,P,D	-	100-177	-	-	-	-	0.0083 ± 0.0005	(490) is likely interloper (Michel et al. 2011)
569	Misa	70	543	0.031	C	88c	117	0.58-0.25	52	−3.9	−2.3	0.5 ± 0.2	
606	Brangane	30	81	0.102	S	37	46	0.92-0.48	22	?	−3.8	0.05 ± 0.04	
668	Dora	50	837	0.054	C	85	165!	0.031-0.004	50	−4.2	−1.9	0.5 ± 0.2	
808	Merxia	50	549	0.227	S	37	121!	0.66-0.018	22	−2.7	−3.4	0.3 ± 0.2	
832	Karin	-	-	-	S	-	40	-	-	-	-	0.0058 ± 0.0002	
845	Naema	30	173	0.081	C	77c	81	0.35-0.30	46	−5.2	−2.9	0.1 ± 0.05	
847	Agnia	40	1077	0.177	S	39	61	0.38-0.10	23	−2.8	−3.1	0.2 ± 0.1	
1128	Astrid	50	265	0.079	C	43c	?	0.52	25	−1.7	−2.6	0.1 ± 0.05	
1272	Gefion	60	19477	0.20	S	74c	100-150!	0.001-0.004	60	−4.3	−2.5	0.48 ± 0.05	Nesvorný et al. (2009), L chondrites
1400	Tirela	80	1001	0.070	S	86	-	0.12	86	−4.2	−3.4	<1.0	
1658	Innes	70	621	0.246w	S	27	?	0.14	16	−4.9	−3.5	<0.7	(1644) Rafita is interloper
1726	Hoffmeister	40	822	0.035	C	93c	134	0.022-0.007	55	−4.5	−2.7	0.3 ± 0.2	
3556	Lixiaohua	60	439	0.044w	C/X	62	220!	0.029-0.001	35	−6.1	−3.3	0.15 ± 0.05	Novaković et al. (2010)
3815	Konig	60	177	0.044	C	33	?	0.32	20	?	−3.0	<0.1	(1639) Bower is interloper
4652	Iannini	-	-	-	S	-	-	-	-	-	-	0.005 ± 0.005	
9506	Telramund	40	146	0.217w	S	22	-	0.05	13	−3.9	−3.7	<0.5	
18405	1993 FY_{12}	50	44	0.171w	C/X	15	-	0.23	15	−2.4	−2.4	<0.2	cut by J5/2 resonance

Table 2. A continuation of Table 1.

designation		v_{cutoff} m/s	N	p_V	tax.	D_{PB} km	D_{Durda} km	LR/PB	v_{esc} m/s	q_1	q_2	age Gyr	notes, references
158	Koronis$_{(2)}$	-	-	-	S	35	-	-	-	-	-	0.015 ± 0.005	cratering, Molnar & Haegert (2009)
298	Baptistina	50	1249	0.160w	C/X	35c	-	0.17	21	−3.6	−2.4	<0.3	part of the Flora family
434	Hungaria	200	4598	0.35	E	25	-	0.15	15	−5.9	−3.1	0.5 ± 0.2	Warner et al. (2010)
627	Charis	80	235	0.081	S	>60	-	0.53	35	?	−3.4	<1.0	
778	Theobalda	85	154	0.060	C	97c	-	0.29	57	?	−2.9	0.007 ± 0.002	cratering, Novaković (2010)
302	Clarissa	30	75	0.054	C	39	-	0.96	23	?	−3.1	<0.1	cratering, Nesvorný (2010)
656	Beagle	24	63	0.089	C	64	-	0.56	38	−1.3	−1.4	<0.2	
752	Sulamitis	60	191	0.042	C	65	-	0.83	39	−6.5	−2.3	<0.4	
1189	Terentia	50	18	0.070	C	56	-	0.990	33	?	−2.6?	<0.2	cratering
1892	Lucienne	100	57	0.223w	S	14	-	0.71	8	?	−4.4	<0.3	
7353	Kazvia	50	23	0.206w	S	16	-	0.57	8	?	−1.8	<0.1	
10811	Lau	100	15	0.273w	S	11	-	0.77	5	?	−2.8	<0.1	
18466	1995 SU_{37}	40	71	0.241w	S	14	-	0.045	7	?	−5.0	<0.3	
1270	Datura	-	-	-	S	-	-	-	-	-	-	0.00045-0.00060	identified in osculating-element space,
14627	Emilkowalski	-	-	-	C/X	-	-	-	-	-	-	0.00019-0.00025	Nesvorný & Vokrouhlický (2006)
16598	1992 YC_2	-	-	-	S	-	-	-	-	-	-	0.00005-0.00025	
21509	Lucascavin	-	-	-	S	-	-	-	-	-	-	0.0003-0.0008	
2384	Schulhof	-	-	-	S	-	-	-	-	-	-	0.0007-0.0009	Vokrouhlický & Nesvorný (2011)
27	Euterpe	70	268	0.260w	S	118c	-	0.998	70	−2.9	−2.2	<1.0	cratering, Parker et al. (2008)
375	Ursula	80	777	0.057w	C	203c	240-280	0.71-0.43	120	−4.1	−2.3	<3.5	old?
1044	Teutonia	50	1950	0.343	S	27-120	-	0.17-0.98	16-71	−3.5	−3.9	<0.5	depends on (5) Astraea membership
1296	Andree	60	401	0.290w	S	17-74	-	0.010-0.95	10-43	?	−2.9(0.5)	<1.0	depends on (79) Eurynome membership
2007	McCuskey	34	236	0.06	C	29	-	0.41	17	?	−5.6	<0.5	overlaps with Nysa/Polana
2085	Henan	54	946	0.200w	S	27	-	0.13	16	−4.2	−3.2	<1.0	
2262	Mitidika	83	410	0.064w	C	49-79c	-	0.037-0.81	26-46	−4.5	−2.2	<1.0	depends on (785) Zwetana membership, (2262) is interloper, overlaps with Juno
2	Pallas	200	64	0.163	B	498c	-	0.9996	295	?	−2.2	<0.5	high-I, Carruba (2010)
25	Phocaea	160	1370	0.22	S	92	-	0.54	55	−3.1	−2.4	<2.2	old? high-I/e, cut by ν_6 resonance, Carruba (2009)
148	Gallia	150	57	0.169	S	98	-	0.058	58	?	−3.6	<0.45	high-I
480	Hansa	150	651	0.256	S	60	-	0.83	35	−4.9	−3.2	<1.6	high-I
686	Gersuind	130	178	0.146	S	52c	-	0.48	40	?	−2.7	<0.8	high-I, Gil-Hutton (2006)
945	Barcelona	110	129	0.248	S	28	-	0.77	16	?	−3.5	<0.35	high-I, Foglia & Masi (2004)
1222	Tina	110	37	0.338	S	21	-	0.94	12	?	−4.1	<0.15	high-I
4203	Brucato	-	-	-	-	-	-	-	-	-	-	<1.3	in freq. space
31	Euphrosyne	100	851	0.056	C	259	-	0.97	153	−4.9	−3.9	<1.5	cratering, high-I, Foglia & Massi (2004)
702	Alauda	120	791	0.070	B	218c	290-330!	0.025	129	−3.9	−2.4	<3.5	old? high-I, cut by J2/1 resonance, satellite (Margot & Rojo 2007)
107	Camilla	?	?	0.054	-	>226	?	?	?	?	?	3.8?	LHB? Cybele region, non-existent today,
121	Hermione	?	?	0.058	-	>209	?	?	?	?	?	3.8?	LHB? Vokrouhlický et al. (2010)

Table 3. A continuation of Table 1.

designation		$v_{\rm cutoff}$ m/s	N	p_V	tax.	$D_{\rm PB}$ km	$D_{\rm Durda}$ km	LR/PB	$v_{\rm esc}$ m/s	q_1	q_2	age Gyr	notes, references
1303	Luthera	100	142	0.043	X	92	-	0.81	54	−3.9	−2.7	<0.5	above (375) Ursula
1547	Nele	20	57	0.311w	X	19	-	0.85	11	?	−2.8(0.3)	<0.04	close to (3) Juno
2732	Witt	60	985	0.260w	S	25	-	0.082	15	−4.0(0.3)	−3.8	<1.0	only part with $\sin I > 0.099$, above (363) Padua
81	Terpsichore	120	70	0.052	C	119	-	0.993	71	?	−4.4	<0.5	cratering, less-certain families in the “pristine zone”
709	Fringilla	140	60	0.047	X	99c	130-140	0.93-0.41	59	−6.2	−1.7	<2.5	old?
918	Itha	140	63	0.23	S	38	-	0.16	22	−2.7	−1.5	<1.5	shallow SFD
5567	Durisen	100	18	0.044w	X	42	-	0.89	25	?	−1.7	<0.5	shallow SFD
5614	Yakovlev	100	34	0.05	C	22	-	0.28	13	?	−3.2	<0.2	
12573	1999 NJ_{53}	40	13	0.190w	C	15	-	0.13	9	?	−2.0(0.5)	<0.6	incomplete SFD
15454	1998 YB_3	50	14	0.054w	C	21	-	0.41	13	?	−1.6(0.3)	<0.5	shallow SFD
15477	1999 CG_1	110	144	0.098w	S	25	-	0.065	14	?	−4.6(0.5)	<1.5	
36256	1999 XT_{17}	60	30	0.210w	S	17	-	0.037	10	?	−1.4(0.5)	<0.3	shallow SFD